

Fe³⁺ paramagnetic ion in α -Al₂O₃ energy levels revisited. Application to a 31 GHz Maser proposal

M. Mrad, P.Y. Bourgeois, Y. Kersalé and V. Giordano¹
 FEMTO-ST Institute, Time and Frequency Dpt., 26 chemin de l'Épitaphe, 25030 Besançon Cedex,
 France^{a)}

(Dated: 8 November 2018)

The molecular structure of a $3d^5$ configuration ion in a trigonal ligand field is theoretically established on the basis of the 252×252 complete energy matrix. The optical absorption and the electron paramagnetic resonance spectra of the Fe^{3+} ion in the sapphire crystal (α -Al₂O₃) have been studied by diagonalizing the complete energy matrix. The calculated results are in very good agreement with previous experimental observations. The strength of the transition probabilities between pairs of the energy levels have been calculated to determine the possibility to achieve a population inversion in the ground state by applying optical pumping to the crystal. Preliminary results based on the computed transition parameters and on the maser rate equations model show that a 31 GHz maser signal can be effectively generated depending on the cryogenic resonator design.

Keywords: Molecular Hamiltonian, Energy-levels, transition parameter, state equations, maser effect

I. INTRODUCTION

Masers based on paramagnetic ions hosted in a crystal were extensively studied and used as stable microwave sources or as low noise amplifiers in the 60's¹. Maser action was obtained at low temperature in different doped crystals, which the most popular was the sapphire doped with Cr³⁺ or Rubis. Numerous types of maser were designed generally based on a doped crystal inserted into a waveguide or a metallic cavity cooled down the liquid Helium temperature. The doping level was typically of the order of 0.05% or so and for a X-band source the cryogenic resonator presented a Q-factor of the order of 10,000 or less. Most of the systems were based on the ground state levels multiplicity to get the required population inversion through the action of a microwave pumping. Some attempts to optically pump the crystal have been realized^{2,3}. But no real advantage compared to the classical maser scheme has been demonstrated. The lack of narrowband and easy to handle laser source as well as the poor quality of available doped crystals were certainly the main difficulties to achieve a reliable optically pumped microwave maser. Eventually the interest for this technology was almost stopped after the development of low noise figure cryogenic semiconductor amplifiers, stable quartz crystal oscillators and low noise frequency synthesis.

More recently, we reported the possibility to get a 12 GHz maser signal presenting a short term relative frequency instability below 1×10^{-14} at short term with a large margin of progress^{4,5}. Such a frequency stability performance is required for a number of very demanding applications as metrology, space navigation, radioastronomy or fundamental physics experiments. The search for a reliable microwave source presenting a relative frequency stability of some 10^{-15} is a challenge that motivates a lot of innovative works all around

the world⁶⁻⁸. In our first prototype the sustaining amplification is achieved in a cryogenic sapphire whispering gallery mode resonator containing a small amount of paramagnetic Fe^{3+} ions. The Fe^{3+} ion exhibits three ground state energy levels. A population inversion is obtained between the two lower ground state levels by submitting the Fe^{3+} ions to a 31 GHz signal. The maser oscillation takes place at 12.04 GHz. As the sapphire resonator exhibits at low temperature extremely low losses, the Fe^{3+} ion concentration required to get enough gain is very low. Contrary to the maser of the 60's, our WhiGMO (Whispering Gallery Maser Oscillator) incorporates a microwave resonator presenting a Q-factor of typically one billion at 4.2K made from a sapphire crystal containing typically 0.1 ppm or less of active ions. The experimental validation of the 12 GHz WhiGMO and its potentiality to be competitive with the state-of-the-art microwave stable references opens the way to revisit the Maser concept and the associated material properties. Moreover the WhiGMO principle can be extended to other transitions of the Fe^{3+} ion in sapphire or to other doped crystals to design stable sources at higher frequencies.

In this paper we refined the description of the Fe^{3+} ion embedded into a (α -Al₂O₃) matrix to derive its 252 energy levels with an improved accuracy compared to previous works⁹. Moreover we calculated the Fe^{3+} ion strength transition probability including those for optical transitions. It appears that a few allowed optical transitions are favorable to obtain a maser operation at 31 GHz applying optical pumping at wavelength achievable with available low cost laser sources. Eventually, a first preliminary evaluation of the 31 GHz maser concept is presented. It is shown that the 31 GHz maser signal power achievable is larger than the classical 12 GHz version, i.e. a power gain of 100 is expected in the optimized conditions. As fundamental limit of frequency stability is fixed by the thermal noise, any increase in the maser signal output will benefit to the performance.

^{a)}Electronic mail: mohamad.mrad@femto-st.fr

II. THE MOLECULAR HAMILTONIAN

The electronic configuration of the Fe^{3+} cation is $[Ar]3d^5$. The spectroscopic term of the ground state is 6S ($S=5/2$ and $L=0$). In a doped sapphire crystal the Fe^{3+} ion replaces the cation Al^{3+} and undergoes the action of the crystal field of the nearby ions O^{2-} and Al^{3+} (figure 1). The cation is located in a distorted octahedral. Assuming the cation Fe^{3+} in symmetry O_h , the fundamental term will be ${}^6A_{1g}(O_h)$.

Since the appearance of the fundamental articles of Racah¹⁰, Eliot and Stevens¹¹ and Judd¹², the theoretical interpretation of electronic spectra of transition metals has become increasingly easy. The appropriate molecular Hamiltonian is:

$$H = H_{ee} + H_{so} + H_c + H_{Zeeman} + Trees\ correction + Racah\ correction \quad (1)$$

In this section, we will discuss the electronic energy levels of a transition metal ion in crystalline solid. The theoretical foundation is already established and discussed in detail in the bibliography¹²⁻¹⁶. The Hamiltonian includes : the electrostatic Coulomb interactions (H_{ee}), the spin-orbit coupling (H_{so}), the ion-ligand interactions described in the framework of crystal field theory (H_c), the Zeeman interaction, and the Trees and Racah corrections.

A. Free ion

Assuming the radial function of the Fe^{3+} d orbital as proposed by Zhao¹⁷ using the "double-zeta exponential" method, we find:

$$R_d(r) = 0.677 \left(\frac{11.2^7}{6!} \right)^{1/2} r^2 \exp(-5.6r) + 0.55237 \left(\frac{3.446^7}{6!} \right)^{1/2} r^2 \exp(-1.732r) \quad (2)$$

From $R_d(r)$, the Racah parameters B_0 and C_0 , the spin-orbit coupling constant ζ_0 , and the mean values $\langle r^k \rangle_0$ have been calculated for the free ion:

$$B_0 = 1130.22\ cm^{-1}, \quad C_0 = 4111.45\ cm^{-1} \\ \zeta_0 = 588.946\ cm^{-1} \quad (3)$$

$$\langle r^2 \rangle_0 = 1.89039\ a.u., \quad \langle r^4 \rangle_0 = 11.46485\ a.u.$$

We take into account the Trees¹⁸ and the Racah¹⁹ corrections. The constant of Trees correction $\alpha_0 = 40\ cm^{-1}$ and the Racah correction $\beta_0 = -131\ cm^{-1}$ are fitted from the spectra of the free ion¹⁷.

B. Crystal field interaction

According Wybourne¹⁴, the potential of the crystal field can be written as a linear combination of irreducible tensor operators C_q^k :

$$H_c = \sum_{kq} B_{kq} C_q^k \quad (4)$$

where B_{kq} are the crystal field parameters. In the case of d-electrons, the allowed values for the integer k are 0, 2, 4 and $-k \leq q \leq +k$.

The structure of the equation (4) is determined by the symmetry of the crystal lattice. For a trigonal field (C_{3v}), the summation contains four terms: B_{20} , B_{40} , B_{43} and B_{4-3} . In the generalized model of the crystal field, the trigonal crystal field parameters B_{kq} were given by Zhao⁹. The values of the reduced matrix elements of tensor operators are published in the book of Nielson and Koster²⁰ for 16×16 matrices. From the Wigner-Eckart theorem we developed our generalized model based on 252×252 matrices.

C. Calculation method

The general expression for the interaction between the central metal ion and ligand orbitals is complex, a reasonable approximation for the electrostatic parameters B and C, the constant of spin-orbit, and the average values $\langle r^4 \rangle$ was made that :

$$B = N^4 B_0, \quad C = N^4 C_0 \\ \zeta = N^2 \zeta_0, \quad \langle r^4 \rangle = N^2 \langle r^4 \rangle_0 \\ \alpha = N^4 \alpha_0, \quad \beta = N^4 \beta_0 \quad (5)$$

where N is the average reduction factor due to the covalency.

In the Al_2O_3 crystal the position of Al^{3+} is defined respectively to the sites of the two nearest cations as schematized in the figure 1.

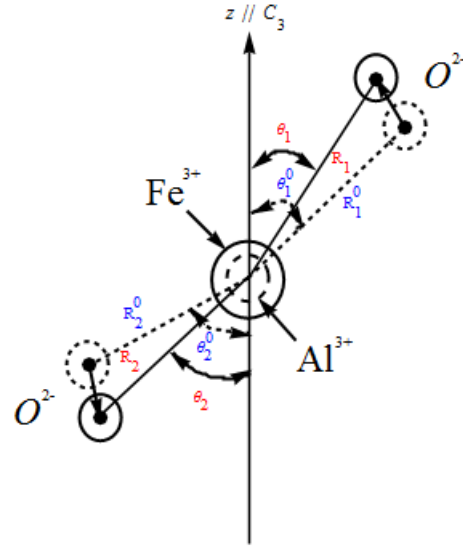


FIG. 1. Local structure distortion of octahedral Fe^{3+} center in $\alpha-Al_2O_3$ system.

The intersite distances and the corresponding angles with respect the symmetry axis C_3 have been determined in previous works^{21,22} as:

$$\begin{aligned} R_1^0 &= 1.966\text{\AA} \quad , \quad \theta_1^0 = 47.44^\circ \\ R_2^0 &= 1.857\text{\AA} \quad , \quad \theta_2^0 = 62.70^\circ \end{aligned} \quad (6)$$

To represent the crystal distortion due to the substitution of Al^{3+} by Fe^{3+} , we assume as proposed by Zhao²³ that the two distances is affected by an identical relative variation. We add an identical constraint to the angle relative variations, thus introducing two independent parameters f and g defined as

$$f = \frac{R_1}{R_1^0} = \frac{R_2}{R_2^0} \quad ; \quad g = \frac{\theta_1}{\theta_1^0} = \frac{\theta_2}{\theta_2^0} \quad (7)$$

Eventually the three independent parameters N, f and g have been varied to approach the experimental observations. We found the optical spectrum of Fe^{3+} in $\alpha-Al_2O_3$ is well represented by taking :

$$N = 0.863 \quad , \quad g = 0.996 \quad \text{and} \quad f = 1.003 \quad (8)$$

The comparison between our calculations and experimental observations is shown in Table I compared to the values given by Zhao⁹, which the method serves as the basis of our own model. The introduction of a third independant adjustable parameter leads to an improvement in the determination of almost all the optical wavelengths in the Fe^{3+} ion spectrum.

To strengthen our confidence in our physical description, we derived from our model the spin-Hamiltonian parameters describing the ground state ${}^6A_1(S)$ of the Fe^{3+} ion. Without applied static magnetic field, there are three energy levels labelled in the following $|i\rangle$ with $i = 1, 2$ or 3 (see figure 2). From the expression of spin-Hamiltonian given in²⁴, the energy difference between the three hyperfine levels of the ground state are written as :

$$E_3 - E_1 = \frac{1}{3}[(18D + a - F)^2 + 80a^2]^{1/2} \quad (9)$$

$$E_2 - E_1 = \frac{3}{2}(a - F) - D + \frac{1}{6}[(18D + a - F)^2 + 80a^2]^{1/2}$$

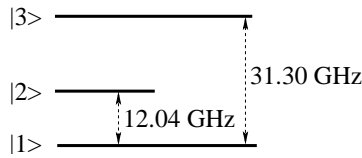


FIG. 2. Structure of Fe^{3+} ground state in the $\alpha-Al_2O_3$ crystal without applied static magnetic field.

The calculated values of the spin-Hamiltonien parameters: $D, a, a-F$ and the energy gaps are given in Table II and compared to the previous evaluation due to Zhao and experimental values.

O_h	Zhao ⁹	This work	Observed ²⁵
${}^4T_1(G)$	9790	9700	9450 - 9700
	10048	9990	
	10229	10128	
	10392	10294	
	10473	10381	
	10493	10396	
${}^4T_2(G)$	14229	14183	14350
	14262	14208	
	14315	14219	
	14373	14256	
	14399	14281	
	14401	14282	
${}^4A_1(G)$	17977	17875	17600 - 17800
	17998	17897	
${}^4E(G)$	18101	18015	
	18143	18056	
	18188	18105	
	18199	18113	
${}^4T_2(D)$	20181	20075	
	20191	20078	
	20341	20233	
	20533	20414	
	20562	20432	
	20823	20470	
${}^4E(D)$	22299	22195	22120 - 22200
	22313	22212	
	22319	22219	
	22328	22229	
${}^4T_1(P)$	25652	25663	25680 - 26700
	25805	25755	
	25945	25875	
	26141	26090	
	26330	26225	
	26457	26526	
${}^4A_2(F)$	30167	29884	29000
	30170	29887	

TABLE I. Calculation and observed of the d-d transition for the crystal $\alpha-Al_2O_3 : Fe^{3+}$ (the values are in cm^{-1}).

ZFS parameters	Zhao 1995 ⁹	This article	Observed ^{26,27}
D	1784	1723	1718 ± 2
a-F	322	330	329 ± 2
a	254	268	241 ± 4
$E_3 - E_1$	10838	10478	10451
$E_2 - E_1$	4118	4011	4015

TABLE II. Calculated spin-Hamiltonian parameters for $\alpha-Al_2O_3 : Fe^{3+}$ at 300 K compared to experimental values (the unit is $10^{-4} cm^{-1}$).

III. TRANSITION PROBABILITY

The optical spectrum of the iron doped sapphire shows fairly intense absorption bands^{25,28} indicating that we can interact optically with the Fe^{3+} ions. Our objective is to evaluate the possibility to get a population inversion in the ground state by applying an optical radiation to the crystal. Thus we need to calculate the effect of an optical radiation on the population of each ground state level $|i\rangle$, with $i = 1, 2$ or 3 taking into account the allowed transitions with the different excited levels $|j\rangle$ listed in the table I. Following Siegman¹ the transition rate W_{ij} between one ground state level $|i\rangle$ and one excited level $|j\rangle$ is given by:

$$W_{ij} = \frac{1}{4}(\gamma H)^2 g(\nu) \sigma^2 \quad (10)$$

Where, γ : the gyromagnetic factor. H : the module of the RF or optical magnetic field. $g(\nu)$: the line shape function describing the spectral broadening of the absorption line.

σ^2 is a dimensionless factor representing the strength of the transition probability, which depends on the relative orientation of the oscillating magnetic field with respect the crystal axis z . σ^2 is computed from the matrix element of the interaction hamiltonian, which depends on the total magnetic momentum and on the applied oscillating magnetic field. In our case where no static magnetic field is present, two different orientations have to be considered: $H \perp z$ or $H // z$. We found that for each transition only one configuration gives noticeable value for σ^2 . In the table III, we give the relevant σ_{ij}^2 parameters for each transition. The relative orientation of H with respect z is indicated by the symbol (\perp) or ($//$).

IV. PROPOSAL FOR A 31 GHZ MASER

Laser sources emitting some 100 mW at 555 nm with a linewidth less than 0.1 nm are currently commercially available (see for ex.²⁹). From the table III we selected the transition to the ${}^4E(G)$ excited level, at 18015 cm^{-1} ($\approx 555 \text{ nm}$). The transition probabilities for the ${}^6A_1(S) \rightarrow {}^4E(G)$ transition with $H \perp z$ are: $\sigma_1^2 = 1.40 \times 10^{-3}$, $\sigma_2^2 = 1.80 \times 10^{-4}$ and $\sigma_3^2 \approx 0$. Thus if we submit the crystal to a narrowband 555 nm laser source, the $|1\rangle$ level will be more effectively pumped, and thus large population differences between $|1\rangle$ and the two other ground state levels can be obtained.

A. Rate equations

Let's consider a Fe^{3+} doped Al_2O_3 crystal submitted to a 555 nm narrowband source resonant with the transition ${}^6A_1(S) \rightarrow {}^4E(G)$. The proposed system is schematized in figure 3. A cylindrical cryogenic sapphire resonator presenting a high-Q resonance mode at 31 GHz is submitted to an optical radiation at 555 nm. The crystal axis z is colinear to the cylinder axis. The 31 GHz resonant mode is assumed to be quasi-transverse magnetic, i.e. the magnetic field lines in

O_h	σ_{1j}^2	σ_{2j}^2	σ_{3j}^2
${}^6A_1(S)$	2.00 (0) [\perp] 3.27 (3) [\perp]	- 1.25 (0) [\perp]	- -
${}^4T_1(G)$	1.84 (6) [$//$] 1.52 (5) [\perp] 8.53 (7) [\perp] 2.17 (5) [\perp] 4.08 (5) [$//$] 1.95 (5) [$//$]	7.43 (5) [\perp] 2.85 (6) [$//$] 1.88 (5) [\perp] 9.90 (5) [$//$] 4.34 (6) [\perp] 8.90 (6) [\perp]	1.70 (6) [\perp] 9.63 (5) [\perp] 1.33 (4) [$//$] 6.19 (6) [\perp] 4.63 (7) [\perp] 3.64 (7) [\perp]
${}^4T_2(G)$	6.87 (4) [$//$] 5.92 (5) [$//$] 5.35 (6) [\perp] 2.97 (5) [\perp] 1.71 (4) [\perp] 1.73 (4) [\perp]	2.08 (4) [\perp] 1.37 (7) [\perp] 2.21 (4) [$//$] 5.56 (4) [\perp] 5.12 (10) [\perp] 4.65 (4) [$//$]	2.74 (4) [\perp] 4.70 (4) [\perp] 1.61 (4) [\perp] 1.43 (4) [$//$] 4.06 (4) [$//$] 1.36 (5) [\perp]
${}^4A_1(G)$	3.43 (3) [$//$] 7.01 (4) [\perp]	1.41 (4) [\perp] 3.24 (5) [$//$]	4.29 (4) [\perp] 1.05 (3) [\perp]
${}^4E(G)$	1.40 (3) [\perp] 1.29 (4) [\perp] 8.88 (4) [$//$] 2.67 (5) [\perp]	1.80 (4) [\perp] 1.16 (3) [\perp] 1.70 (3) [\perp] 4.62 (3) [$//$]	8.32 (4) [$//$] 1.83 (3) [$//$] 6.70 (4) [\perp] 1.26 (3) [\perp]
${}^4T_2(D)$	5.55 (5) [$//$] 6.96 (6) [\perp] 4.50 (5) [\perp] 1.39 (6) [$//$] 7.80 (5) [\perp] 4.73 (5) [$//$]	2.23 (5) [\perp] 7.68 (6) [$//$] 4.93 (5) [\perp] 8.22 (6) [\perp] 2.42 (4) [$//$] 9.33 (7) [\perp]	2.90 (5) [\perp] 5.84 (5) [\perp] 1.62 (4) [$//$] 1.01 (5) [\perp] 2.90 (5) [\perp] 8.77 (5) [\perp]
${}^4E(D)$	9.67 (8) [$//$] 9.12 (9) [\perp] 2.29 (7) [\perp] 2.23 (8) [\perp]	2.80 (7) [\perp] 5.53 (7) [\perp] 1.11 (7) [$//$] 7.54 (8) [\perp]	2.31 (8) [\perp] 7.05 (7) [$//$] 1.80 (7) [\perp] 4.09 (7) [$//$]
${}^4T_1(P)$	1.27 (5) [$//$] 4.15 (6) [$//$] 3.14 (5) [$//$] 4.22 (9) [\perp] 2.35 (6) [$//$] 9.36 (7) [$//$]	1.71 (7) [\perp] 5.79 (7) [\perp] 1.31 (5) [\perp] 6.69 (6) [$//$] 2.19 (5) [\perp] 1.61 (7) [\perp]	6.22 (7) [\perp] 2.58 (8) [\perp] 8.33 (7) [\perp] 4.27 (5) [\perp] 5.23 (8) [\perp] 1.59 (8) [\perp]
${}^4A_2(F)$	2.10 (8) [\perp] 1.20 (7) [$//$]	6.58 (7) [$//$] 6.33 (11) [\perp]	2.63 (7) [\perp] 2.90 (7) [\perp]

TABLE III. Strength of transition probability σ^2 for the Fe^{3+} d-d transitions in $\alpha-Al_2O_3$. The integer (n) in brackets is for $\times 10^{-n}$.

the equatorial plane of the cylinder are perpendicular to the z axis. A small magnetic loop placed near the dielectric cylinder is used to derive the 31 GHz maser signal output.

The excited levels decay rapidly to the ground state with a lifetime $\tau_0 \ll 1$ ms. All relaxation in the ground state are governed by the spin-lattice effect with a characteristic time $\tau_1 \approx 10$ ms at 4 K. It is also well established that the spin-to-spin relaxation is very fast with a characteristic time $\tau_2 \leq 20$ ns. In this case a simple rate equations model dealing only

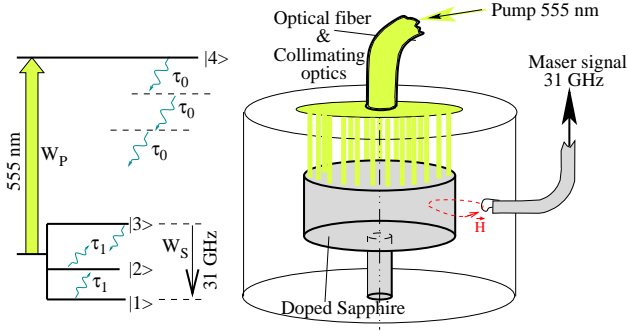


FIG. 3. Energy levels and schematic of the cryogenic optically pumped 31 GHz WhiGMO .

with the level populations and neglecting coherences is sufficient to describe the interaction³⁰. Excited ions can possibly fall on intermediate levels, nevertheless as $\tau_0 \ll \tau_1$ they relax rapidly to ground state. This allows us to only consider a four levels system, i.e. the three ground state levels and the ${}^4E(G)$ excited one, which is labelled $|4\rangle$. The ground state ions submitted to the optical radiation will be excited with an absorption rate W_P , which is evaluated from equation 10. The optical pumping offers the possibility to get a population inversion between $|3\rangle$ and $|1\rangle$ and thus to obtain a maser effect at 31 GHz providing the resonator has been designed to present a high Q resonance at this frequency. The first 31 GHz emitted photons will stimulate others emissions with a rate W_S . If the optical pumping is effective enough to compensate for the resonator loss, a 31 GHz self-sustained oscillation will occur. To theoretically determine the conditions to get a 31 GHz maser signal we followed the method described in³¹ and validated in the case of 12 GHz WhiGMO. The stationary solutions of the rate equations are :

$$\Delta n_{13} = \frac{27\Delta N_{13} + 6(2\Delta N_{13} - 3\Delta N_{14})\tau_1 W_P}{9(3 + 4\tau_1 W_S) + 4(3 + \tau_1 W_S)\tau_1 W_P} \quad (11a)$$

$$\Delta n_{14} = \frac{9(3\Delta N_{14} + 2(2\Delta N_{14} - \Delta N_{13})\tau_1 W_S)}{9(3 + 4\tau_1 W_S) + 4(3 + \tau_1 W_S)\tau_1 W_P} \quad (11b)$$

ΔN_{ij} and Δn_{ij} are the population difference between levels $|i\rangle$ and $|j\rangle$ at the thermal equilibrium and in presence of the pump and maser signal respectively. The pump and maser signal frequencies are denoted ν_{14} and ν_{13} respectively.

B. Threshold pump power

In the absence of the maser signal, the threshold pump power is achieved when the population inversion takes place. The absorption rate W_{P_0} corresponding to this situation is found by making $\Delta n_{13} = 0$ in the equation (11a):

$$W_{P_0} = \frac{9}{2\tau_1} \frac{\Delta N_{13}}{3\Delta N_{14} - 2\Delta N_{13}} \quad (12)$$

The total absorbed power is written as:

$$\begin{aligned} P_0 &= h\nu_{14} W_{P_0} \Delta n_{14_0} N V_{eff} \\ &= \frac{3}{2\tau_1} h\nu_{14} \Delta N_{13} N V_{eff} \end{aligned} \quad (13)$$

N is the Fe^{3+} ions concentration and V_{eff} is the volume occupied by the active ions participating to the maser signal. V_{eff} is the volume of the 31 GHz mode in the sapphire resonator (see section IV D). Here, we assume the optical radiation only lights the resonator part where the 31 GHz mode is concentrated. P_0 is thus the minimal optical power required to get maser action in optimized conditions.

C. Maximum maser signal power

Δn_{13} and thus the 31 GHz signal power increase with the pump signal power system until saturation of the optical transition occurs, i.e. $n_4 \simeq n_1$. Assuming we already overtook this situation, i.e. $W_P \rightarrow \infty$, equations (11) simplify and the maximum maser power is derived as:

$$\begin{aligned} P_{31_{max}} &= h\nu_{13} \text{Max}[W_S \Delta n_{13}] N V_{eff} \\ &= \frac{3}{2\tau_1} h\nu_{13} (3\Delta N_{14} - 2\Delta N_{13}) N V_{eff} \end{aligned} \quad (14)$$

$P_{31_{max}}$ is the total power generated by the active ions inside the resonator. The coupling loop derive only a fraction of this power, which depends on the coupling coefficient β related to the loop area and to its position with respect to the sapphire resonator. For a critical coupling, i.e. $\beta = 1$, the maser output power is one half of $P_{31_{max}}$. The resonator Q-factor is also impacted by the loading to the external circuit and for $\beta = 1$, the loaded Q-factor is one half of the unloaded one.

D. Resonator design

Our objective is to use the Fe^{3+} ions present as contaminant in a high purity sapphire monocrystal. Typical effective ions concentration in such a type a crystal is well below 1 ppm. Thus the 31 GHz resonator has to present a very high quality factor, otherwise the 31 GHz stimulated emissions wont be sufficient to compensate for the resonator loss. This can be accomplished by using a whispering gallery mode, which Q-factor is only limited by the sapphire losses. Quasi-TM Whispering gallery modes are characterized by three integers m, n, l representing the electromagnetic field component variations along the azimuthal, radial and axial directions respectively³². In the following we consider only the resonant modes with low radial and axial variations, i.e. those corresponding to $n = l = 0$. At low temperature, i.e. near the liquid helium temperature, the whispering gallery mode Q-factor can be as high as 1 billion providing the mode order is sufficiently high, i.e. $m > 15$ ³³. The WhiGMO principle has been demonstrated at 12 GHz, i.e. the frequency of the $|1\rangle \rightarrow |2\rangle$

transition. In this case, the population inversion results from a pumping at 31 GHz. The resonator has a diameter $2R = 50$ mm and a thickness $h = 30$ mm. The quasi-TM Whispering Gallery mode $WGH_{17,0,0}$ is used to support the maser signal³⁴.

For the whispering gallery mode the electromagnetic fields are concentrated near curved air-dielectric interface, between the resonator radius R and a caustic of radius R_C . The effective volume $V_{eff} = \pi h (R^2 - R_C^2)$ occupied by the mode is a little mode dependant as R_C is given by:

$$R_C = \frac{m}{\sqrt{\epsilon_r \left(\frac{v_{13}}{c}\right)^2 - \left(\frac{\pi}{2h}\right)^2}} \quad (15)$$

where $\epsilon_r \approx 9.4$ is the sapphire permittivity is the transverse direction with respect z . c the light velocity in vacuum.

To design a 31 GHz resonator we keep the same ratio diameter/thickness, which is near the optimal value³⁵. Thus to design the cryogenic resonator only means choosing the azimuthal number for the mode supporting the 31 GHz signal. m has to be higher than 15 to prevent radiation losses which limit the Q-factor and should not be too high otherwise the coupling with the output probe will be difficult to adjust. The table IV gives for different values of m , the resonator diameter $2R$, the threshold optical power P_0 and the maximum maser power emitted by the ions. Here, the Fe^{3+} concentration is assumed to be 0.02 ppm, i.e. the same value than the 12 GHz WhiGMO.

m	$2R$ (mm)	P_0 (mW)	$P_{31,max}$ (μ W)
17	19.22	1.17	1.02
19	21.13	1.42	1.24
21	23.05	1.71	1.49
25	26.88	2.35	2.05
35	36.46	4.40	3.85
49	50.00	8.41	7.36

TABLE IV. Different resonator designs to support the 31 GHz signal. The pump threshold power P_0 and the maximum maser power $P_{31,max}$ are given for few azimuthal numbers as well as the resonator diameter assuming a constant ratio $\frac{2R}{h} = \frac{5}{3}$.

¹A. E. Siegman, Microwave Solid State Masers, New York : McGraw-Hill (1964).

²J.P. Gayga and J. Hervé, Revue de Physique Appliquée, 6, p. 177-179, June 1971.

- ³D.P. Devor, I.J. D'Haenens and C.K. Asawa, Phys. Review Letters, 8, 11, p. 432-435, June 1, 1962.
- ⁴P. Y. Bourgeois, N. Bazin, Y. Kersalé, V. Giordano, M. E. Tobar, and M. Oxborrow, Applied Physics Letters 87(22), 224104-1-3 (2005).
- ⁵Benmessai K., Bourgeois P.Y., Kersalé Y., Bazin N., Tobar M.E., Hartnett J. G., Oxborrow M, and Giordano V., 2007, Electron. Lett., 43, 1436.
- ⁶V. Giordano, S. Grop, B. Dubois, P.-Y. Bourgeois, Y. Kersalé, G. Cabodevila, E. Rubiola, and G. Haye, Proc. of the 3rd International Colloquium - Scientific and Fundamental Aspects of the Galileo Programme, 31 August - 2 September 2011, Copenhagen, Denmark.
- ⁷T. Kessler, C. Hagemann, T. Legero, U. Sterr, F. Riehle, M. Martin and J. Ye. Proc. of the 2011 Joint Conf. of the IEEE International Frequency Control Symposium and The European Frequency and Time Forum, May 1-5, 2011 San Fransisco, California, USA, p. 699-700.
- ⁸M. J. Thorpe, L. Rippe, T. M. Fortier, M. S. Kirchner and T. Rosenband, Nature Photonics, 5, 688-693, (2011)
- ⁹M. G. Zhao and M. Chui, Phys. Rev. B 52 (1995).
- ¹⁰G. Racah, Phys. Rev. 62, 438 (1942); 63, 367 (1943); 76, 1352 (1949); 85, 381 (1952).
- ¹¹R. J. Elliot and K. W. H. Stevens, Proc. Roy. Soc. A218, 553 (1953); A219, 387 (1953); A65, 209 (1963).
- ¹²B. J. Judd, Second Quantization and Atomic Spectroscopy, John Hopkins University Press (1967).
- ¹³B. R. Judd, Operator techniques in atomic spectroscopy (1963).
- ¹⁴B. G. Wybourne, Spectroscopic properties of rare earths (1965).
- ¹⁵A. Abragam and B. Bleaney, Electron paramagnetic resonance of transition ions (1986).
- ¹⁶G. Liu and B. Jacquier, Spectroscopic properties of rare earths in optical materials (2005).
- ¹⁷M. G. Zhao and M. Chui, Phys. Rev. B 49, 12556 (1994).
- ¹⁸R. E. Trees, Phys. Rev. 85, 6 (1951); Phys. Rev., 83-4 (1951); Phys. Rev., 123-4 (1961)
- ¹⁹G. Racah, Phys. Rev. 83, 4 (1951).
- ²⁰C. W. Nielson and G. F. Koster, Spectroscopic Coefficients for the p^n , d^n and f^n Configurations Cambridge, Massachusetts (1963).
- ²¹D. S. MacClure, J. Chem. Phys. 38, 2289 (1963).
- ²²K. Moorjani, N. Moorjani, and N. Meavoy, Phys. Rev. 132, 504 (1963).
- ²³M. G. Zhao, Chemical-Physics 18, 109 (1998).
- ²⁴B. Bleaney and al., Reports on Progress in Physics (1953).
- ²⁵G. Lemann and H. Harder, Am. min. 55, 98 (1970).
- ²⁶G. S. Bogle and H. F. Symmons, Proc. Phys. Soc. 73, 531 (1959).
- ²⁷S. Lee, C. M. Brodbeck and C. Yang, Phys. Rev. B 15, 2469 (1977).
- ²⁸G. Lemann, Am. min. 56 (1971).
- ²⁹www.crystalaser.com.
- ³⁰M. Mrad, P.-Y. Bourgeois, M.E. Tobar, Y. Kersalé, V. Giordano, Eur. Phys. J. - AP, accepted for publication, jan. 2, 2012.
- ³¹K. Benmessai, P. Y. Bourgeois, M. E. Tobar, N. Bazin, Y. Kersalé, and V. Giordano, Meas. Sci. Technol., 21, 025902 (2010).
- ³²X.H. Jiao, P. Guillon, L.A. Bermudez, IEE Proc., 154, p. 497-501 (1987)
- ³³P.Y. Bourgeois, Y. Kersalé, N. Bazin, M. Chaubet, and V. Giordano, IEEE Trans. onUFFC, 51, 10, p.1232-1239 Oct. 2004
- ³⁴P.-Y. Bourgeois, M. Oxborrow, M. E. Tobar, N. Bazin, Y. Kersalé and V. Giordano. Int. J. of Modern Physics B, 20, n 11-12 & 13, may 20, 2006, pp. 1606-1612.
- ³⁵J. Krupka, D. Cros, A. Luiten and M. Tobar, Electronics Letters, 32, n 7, p. 670-671, March 28, 1996.